Collisionless motion of neutral particles in magnetostatic traps

Surkov, E.L.; Walraven, J.T.M.; Shlyapnikov, G.V.

DOI
10.1103/PhysRevA.49.4778
Publication date
1994

Published in
Physical Review A

Collisionless motion of neutral particles in magnetostatic traps

E.L. Surkov,[1] J.T.M. Walraven,[2] and G.V. Shlyapnikov[1,2]
[1] *Russian Research Center Kurchatov Institute, Kurchatov Square, 123182 Moscow, Russia*
[2] *Van der Waals–Zeeman Laboratory, University of Amsterdam Valckenierstraat 65-67, 1018 XE Amsterdam, The Netherlands*
(Received 27 December 1993)

We present an analytical and numerical analysis of collisionless motion of neutral particles in magnetostatic traps. We treat the example of an idealized Ioffe quadrupole trap, emphasizing that the essential features of coupling between the degrees of freedom are of general relevance for static traps. In common situations the coupling between axial and radial motion predominantly occurs in a regular way. The coupling is weak, in particular, when the frequency of axial oscillations Ω_z is much smaller than the radial frequency Ω_ρ and the particle energy is much lower than the Zeeman energy in the center of the trap. Then, under an adiabatic change of the potential parameters, the quantity $\mathcal{E}_z/\Omega_z$, where $\mathcal{E}_z$ is a characteristic axial energy, is an approximate adiabatic invariant. If Ω_z is decreasing and Ω_ρ is constant, then the characteristic radial energy $\mathcal{E}_\rho$ will remain constant while $\mathcal{E}_z$ decreases proportionally to Ω_z. This implies one-dimensional adiabatic cooling, which is an interesting option for gravitational studies of light atoms such as hydrogen and antihydrogen.

PACS number(s): 32.80.Pj, 07.65.−b, 36.10.−k

I. INTRODUCTION

The collisionless motion of neutral particles in magnetostatic traps is of great interest for studies with ultracold atoms. Magnetostatic traps are characterized by the presence of a magnetic field minimum near which atoms with magnetic moment antiparallel to the field can be localized. The presence of saddle points in the potential energy profile allows atoms to escape from the trap. A quantity of principal importance for trapped gases is the ratio between the particle mean free path λ and the characteristic size of a gas sample, L. At densities currently investigated we have

$$\lambda \gg L. \tag{1}$$

Under this condition many interesting phenomena involving the nonlinear dynamics of particle collisionless motion occur on a time scale short compared to the characteristic collisional time. This applies, for example, to optical cooling with a single light beam or time evolution of the distribution of trapped atoms in momentum and coordinate space [1,2]. These phenomena find their origin in the nonlinear coupling between the degrees of freedom. This coupling also determines the possibility of one-dimensional adiabatic cooling [3], which is an interesting option to cool light atoms, such as hydrogen and antihydrogen [4], to extremely low energies of motion in the vertical direction (< 1 mK), as desired for gravity experiments in the earth gravitational field.

Remarkably, the condition (1) can also hold at densities and temperatures required for observing Bose-Einstein condensation (BEC) and related macroscopic quantum phenomena in trapped gases. It means that with regard to BEC at least two aspects of the particle collisionless motion are important. The first one is the relation between particle motion and Majorana spin flips (see [5]) which limit the attainment of BEC. Also important is the influence of nonlinear dynamics on the escape of particles during evaporative cooling or during a measurement of the energy distribution function of trapped particles by rapidly ramping down a confining barrier [1].

Some magnetostatic traps, such as the two-coil quadrupole trap, have axial symmetry. For Ioffe or baseball traps this symmetry is absent [6]. Ioffe traps are attractive, especially for achieving the BEC, as they represent a flexible geometry in which the Majorana depolarization can be effectively suppressed by choosing a nonzero field at the trap minimum. In magnetostatic traps one may expect regular coupling between the degrees of freedom (see [7]) as well as mixing which leads to chaotic motion. Both features are important for the problems mentioned above.

In this paper we analyze, both analytically and numerically, the collisionless classical motion of trapped atoms for the case of an idealized Ioffe quadrupole (IQ) trap. We emphasize that the essential features of coupling between the degrees of freedom are relevant for any static trap. The most common situation corresponds to substantial regular coupling between the degrees of freedom. At sufficiently low energies the coupling between axial and radial motion can be very weak as near the trap minimum the coupling terms in the trapping potential (the terms containing a product of powers of axial and radial coordinates) are small. For energies close to the potential energy value at the saddle points the motion can become chaotic. Accordingly, we distinguish three energy regions, corresponding to weak axial (z)-radial (x,y) coupling, strong regular coupling, and chaotic motion. The motions in the x and y directions are always strongly coupled. Weak coupling between axial and radial motion appears, in particular, when the oscillation frequency in the axial direction, Ω_z, is much smaller than the frequency of radial oscillations, Ω_ρ, and the particle energy is much smaller than the Zeeman energy in the center of the trap. In this case an adiabatic change of the param-

eters of the trapping potential leaves the ratio $\mathcal{E}_z/\Omega_z$ ($\mathcal{E}_z$ is the characteristic axial energy of the particle) approximately unchanged, i.e., this ratio is an approximate adiabatic invariant. Hence, for an adiabatically decreasing axial frequency the axial energy decreases as Ω_z, which implies one-dimensional adiabatic cooling.

II. IDEALIZED IOFFE QUADRUPOLE TRAP: HAMILTONIAN AND EQUATIONS OF MOTION

The IQ trap consists of four straight conductors ("Ioffe bars"), symmetrically arranged around the z axis and carrying currents in alternating directions to produce a quadrupole field, and further two dipole coils, having the z axis as a common symmetry axis and biased with parallel currents. The IQ trap has been used for plasma confinement [8] and, with a homogeneous field superimposed along the symmetry axis, for neutral atom trapping as originally proposed by Pritchard [9]. In this type of trap, described in some detail in Ref. [6], the magnetic field profile near the origin is given by

$$\begin{aligned} B_\varrho &= \alpha\varrho\cos 2\Phi + \beta Z\varrho\,, \\ B_\Phi &= \alpha\varrho\sin 2\Phi\,, \\ B_Z &= B_0 + \beta(Z^2 - \varrho^2/2)\,, \end{aligned} \tag{2}$$

where Z, ϱ, and Φ are cylindrical coordinates. The collisionless motion of a neutral particle with mass m and magnetic moment $\boldsymbol{\mu}$ antiparallel to the field is described by the Hamiltonian

$$\begin{aligned} \mathcal{H} &= \mathbf{P}^2/2m + \mathcal{U}(\mathbf{R}), \\ \mathcal{U}(\mathbf{R}) &= \mu\,[B(\mathbf{R}) - B_0]\,, \end{aligned} \tag{3}$$

where $\mathbf{P}$ is the particle momentum and $\mathbf{R} = \{X, Y, Z\}$, $\mathcal{U}(\mathbf{R})$ are the position vector and potential energy both defined with respect to the center of the trap. The modulus of the magnetic field

$$\begin{aligned} B(\mathbf{R}) = [&(B_0 + \beta Z^2)^2 \\ &+ (\alpha^2 - \beta B_0 + 2\alpha\beta Z\cos 2\Phi)\varrho^2 + \tfrac{1}{4}\beta^2\varrho^4]^{1/2}\,. \end{aligned} \tag{4}$$

Introducing a characteristic length, frequency, and energy

$$l_c = \frac{\alpha}{\beta}\,,\quad \Omega_c = \left[\frac{\mu\beta}{m}\right]^{1/2},\quad \mathcal{E}_c = \mu\frac{\alpha^2}{\beta} \tag{5}$$

and turning to dimensionless coordinates, momenta, and time

$$\mathbf{r} = \frac{\mathbf{R}}{l_c}\,,\quad \mathbf{p} = \frac{\mathbf{P}}{m l_c \Omega_c}\,,\quad \bar{t} = \Omega_c t \tag{6}$$

we can reduce the Hamiltonian to the form

$$H = \mathbf{p}^2/2 + U(\mathbf{r}) \quad \text{with } \mathcal{H} = H\mathcal{E}_c, \tag{7}$$

where, in Cartesian coordinates,

$$\begin{aligned} U(x,y,z) = [&(b + z^2)^2 + (1-b)(x^2+y^2) \\ &+ \tfrac{1}{4}(x^2+y^2)^2 + 2(x^2-y^2)z]^{1/2} - b \end{aligned} \tag{8}$$

and

$$b = \mu B_0/\mathcal{E}_c. \tag{9}$$

Equations (2), (4), and (8) are valid for $R \ll R_0$, where R_0 is the characteristic dimension of the trap configuration (the coil radius, the distance between coils, the distance from the Ioffe bars to the axis). For a typical IQ trap as used in experiments [1,10], the characteristic length $l_c \gg R_0$ and, hence, these equations apply only close to the origin, i.e., for $r \ll 1$. However, traps with $l_c \ll R_0$ are also conceivable. Then, Eq. (8) also describes the field profile at $r \gg 1$, including saddle points and new elliptic points.

We refer to the trap configuration expressed by Eq. (8) as the idealized IQ trap. A contour plot of the potential shape is shown in Fig. 1 for $b = 0$ and 0.1 and a section along the y, z plane. Notice that for this idealized trap the reduced expression for the potential, Eq. (8), only contains a single free parameter b which determines the 'elongation' of the potential well. In view of Eq. (7) this allows us to describe the particle motion in the idealized IQ trap, and also near the minimum of *any* IQ trap, with just two parameters: the dimensionless magnetic field at the origin, b , and the dimensionless energy $E = \mathcal{E}/\mathcal{E}_c$, where $\mathcal{E}$ is the total energy. To distinguish between various regimes of particle motion the ratio between the axial and radial energies is also important. In dimensionless variables (6) the equations of motion are governed by the Hamiltonian H. From this point on we work with dimensionless quantities unless otherwise stated.

Trapping near the origin can occur only for $b < 1$ and provided the particle energy is sufficiently small (see, e.g., [6]). The Hamiltonian (7) is invariant under the group $\hat{g}$ of point transformations

$$\hat{g} = \{x \to -x\}, \{y \to -y\}, \{z \to -z, x \to y\} \tag{10}$$

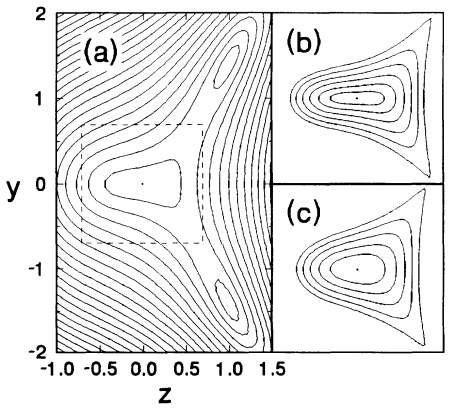

FIG. 1. Contour plots of the potential energy profile $U(x,y,z)$ for the idealized IQ trap: (a) showing the elliptic points and saddle points in the y,z plane for $b = 0$ and contour spacing $\Delta U = 0.2$, (b) central part for $b = 0$ and $\Delta U = 0.05$; (c) central part for $b = 0.1$ and $\Delta U = 0.05$.

and has several singular points. There is an elliptic point at the trap center, $\{x, y, z\} = \{0, 0, 0\}$, and four other elliptic points, i.e.,

$$\{0, \sqrt{2(b+1)}, 1\} \tag{11}$$

and those obtained from (11) by the transformation $\hat{g}$. There are also four saddle points crossed by a separatrix of the phase space:

$$\hat{g}\ \{0, (2b - 4 + 2\sqrt{5-4b})^{1/2}, \tfrac{1}{2}(\sqrt{5-4b} - 1)\}. \tag{12}$$

When $b \to 1$ the saddle points (12) approach the trap center.

In this paper we consider only the case $b < 1$ with particle energies lower than the potential energy value at the saddle points, which corresponds to trapping in the central region of the trap. In the limit

$$E \ll b \tag{13}$$

we can expand Eq. (8) in powers of the coordinate variables. Retaining only the quadratic, cubic, and fourth-power terms we obtain

$$U = \tfrac{1}{2}\omega_z^2 z^2 + \tfrac{1}{2}\omega_\rho^2 \rho^2 + \tilde{A}(x^2 - y^2)z - \tilde{B}\rho^2 z^2 - \tilde{C}\rho^4, \tag{14}$$

where $\rho = \left(x^2 + y^2\right)^{1/2}$, the dimensionless axial and radial frequencies $\omega_z = \Omega_z/\Omega_c$, $\omega_\rho = \Omega_\rho/\Omega_c$ are given by

$$\omega_z = \sqrt{2}\ ,\ \omega_\rho = \sqrt{(1-b)/b}, \tag{15}$$

and the dimensionless nonlinear parameters by

$$\begin{aligned} \tilde{A} &= \frac{\omega_z^2 \omega_\rho}{2\sqrt{b(1-b)}} = \frac{1}{b}\,, \\ \tilde{B} &= \frac{\omega_z^2 \omega_\rho^2}{4b} = \frac{(1-b)}{2b^2}\,, \\ \tilde{C} &= \frac{\omega_\rho^4 (1-2b)}{8b(1-b)^2} = \frac{(1-2b)}{8b^3}. \end{aligned} \tag{16}$$

When

$$b \ll 1 \tag{17}$$

the condition (13) causes the fourth-power terms in the expansion (14) to be much smaller than the quadratic ones. The parameters

$$\varepsilon_z = E_z/b \ll 1\ ,\ \varepsilon_\rho = E_\rho/b \ll 1 \tag{18}$$

determine the characteristic ratios of the $\rho^2 z^2$ term to the ρ^2 and z^2 terms, respectively, and ε_ρ also determines the ratio of the ρ^4 term to the ρ^2 one. The cubic term is small compared to the quadratic terms when the condition

$$\varepsilon = \frac{\omega_z E_\rho}{\omega_\rho \sqrt{E_z b}} = \sqrt{2} E_\rho E_z^{-1/2} \ll 1 \tag{19}$$

is satisfied. Here E_z and E_ρ are characteristic energies of the particle motion in the axial (z) direction and normal to the z axis, respectively (the characteristic values of the coordinates are $z \sim E_z^{1/2}/\omega_z$, $\rho \sim E_\rho^{1/2}/\omega_\rho$). For $E_\rho \sim E_z$ the criterion (19) is definitely fulfilled under the conditions (13) and (17). So, under these conditions the potential (14) corresponds to a three-dimensional linear oscillator with small nonlinear interaction between the degrees of freedom.

The condition $b \ll 1$ corresponds to slow axial motion as compared to the radial one:

$$\omega_z \ll \omega_\rho. \tag{20}$$

At constant z the first fourth-power term ($\sim z^2\rho^2$) leads to equal frequency shifts for x and y motion. The cubic term makes these frequencies slightly different, and only the second fourth-power term makes the radial motion nonlinear. As the x and y oscillations are almost at resonance, the x, y motion can be represented by a fast motion along an ellipse which slowly rotates and changes its eccentricity.

Further analysis is best done in terms of angle-action variables by using the canonical transformation

$$z = (2J_z/\omega_z)^{1/2} \sin\phi_z\ ,\ p_z = (2\omega_z J_z)^{1/2} \cos\phi_z \tag{21}$$

for the z motion and similar ones for the x and y motion. Using the transformation

$$\begin{aligned} J_x &= J_\phi/2 + J_\psi\ ,\ J_y = J_\phi/2 - J_\psi\,, \\ \phi_x &= \phi + \psi/2\ ,\ \phi_y = \phi - \psi/2\,, \end{aligned} \tag{22}$$

the radial motion can be divided into fast ϕ motion along the ellipse and slow ψ motion which describes its deformation. In new variables the Hamiltonian H takes the form

$$\begin{aligned} H = {} & \omega_z J_z + \omega_\rho J_\phi + A J_z^{1/2} \sin\phi_z \left[2J_\psi \left(\sin^2\frac{\psi}{2} + \sin^2\phi\cos\psi\right) + \frac{1}{2}J_\phi \sin 2\phi \sin\psi\right] \\ & -2BJ_z \sin^2\phi_z \left[J_\phi \left(\sin^2\frac{\psi}{2} + \cos\psi\sin^2\phi\right) + J_\psi \sin 2\phi \sin\psi\right] \\ & -8C\left[J_\phi^2 \left(\sin^2\frac{\psi}{2} + \sin^2\phi\cos\psi\right)^2 + 2J_\phi J_\psi \sin 2\phi \sin\psi \left(\sin^2\frac{\psi}{2} + \sin^2\phi\cos\psi\right) + J_\psi^2 \sin^2 2\phi \sin^2\psi\right]. \end{aligned} \tag{23}$$

For $b \ll 1$ we have

$$A = \omega_z \left[\frac{2\omega_z}{b}\right]^{1/2}, \quad B = \frac{\omega_\rho \omega_z}{2b}, \quad C = \frac{\omega_\rho^2}{16b}. \tag{24}$$

The analysis of the equations of motion for the Hamiltonian (23) is a difficult task. It can be simplified by introducing an averaging procedure (see, e.g., [11]). If the ϕ motion is fast in comparison to the z and ψ motion, which is the case for $\omega_z \ll \omega_\rho$, Eq. (23) may be averaged over the fast variable ϕ. This yields

$$\begin{aligned}\tilde{H} = {} & \omega_z J_z + \omega_\rho J_\phi + A J_z^{1/2} J_\psi \sin\phi_z - B J_\phi J_z \sin^2\phi_z \\ & + C(J_\phi^2 - 4J_\psi^2)\sin^2\psi - 3C J_\phi^2 ,\end{aligned} \tag{25}$$

and the equations of motion at constant parameters of the trapping potential become

$$\begin{aligned}\dot{J}_\phi &= 0, \\ \dot{\phi} &= \omega_\rho - B J_z \sin^2\phi_z - 2C J_\phi (3 - \sin^2\psi), \\ \dot{J}_z &= -A J_\psi J_z^{1/2} \cos\phi_z + B J_z J_\phi \sin 2\phi_z, \\ \dot{\phi}_z &= \omega_z + \tfrac{1}{2} A J_\psi J_z^{-1/2} \sin\phi_z - B J_\phi \sin^2\phi_z, \\ \dot{J}_\psi &= -C(J_\phi^2 - 4J_\psi^2)\sin 2\psi, \\ \dot{\psi} &= A J_z^{1/2} \sin\phi_z - 8C J_\psi \sin^2\psi.\end{aligned} \tag{26}$$

Note that averaging the equations of motion that follow directly from Hamiltonian (23) leads to the same result.

In accordance with Kolmogorov-Arnold-Moser theory (see, e.g., [11]) the averaging procedure is valid at least up to times $\bar{t} \sim 1/\omega\eta$ where ω is the characteristic frequency and η is a small parameter determining the ratio of the perturbation (the nonlinear terms in our case) to the leading terms of the Hamiltonian ($\omega_z J_z$ and $\omega_\rho J_\phi$). In our case we obtain that the equations for J_z and ϕ_z are valid at least up to $\bar{t} \sim \min[1/(\omega_z\varepsilon), 1/(\omega_z\varepsilon_\rho)]$ and the equations for J_ϕ and ϕ at least up to $\bar{t} \sim \min[1/(\omega_z\varepsilon_z^{1/2}), 1/(\omega_\rho\varepsilon_\rho)]$. Here it should be emphasized that $1/\omega\eta$ is only a lower limit for the times of validity of the averaging procedure. Actually, these times can be much larger.

III. REGULAR COUPLING BETWEEN AXIAL AND RADIAL MOTION

The particle motion in the idealized IQ trap exhibits, like almost any nonlinear motion, stochastic behavior in certain regions of its phase space and the space of potential parameters, yet the particle motion is mostly regular. The stochastic regions are well defined. Chaos is related to the vicinity of separatrices, trajectories in the phase space, which cross saddle points (see, e.g., [12]). In the absence of external perturbations the stochastization is caused by the interaction between the degrees of freedom. Close to a saddle point, where the dwell time of a particle is very long, even small changes in frequency due to this interaction may result in considerable changes in phase. This is the cause of local instability and stochastization.

In the idealized IQ trap the motion becomes chaotic for energies E close to the potential energy value at the saddle points, $E_s(b)$. With increasing b the characteristic energy E_s decreases monotonously from $E_s = 0.3$ at $b = 0$ to $E_s \approx (1-b)^2/2$ for $b \to 1$. As our analysis shows, the relative width $\delta E/E_s$ of the energy interval where chaotic motion occurs is of the order of a few percent for $b \ll 1$ and decreases when b approaches 1.

We emphasize that realistic IQ traps, such as those used in experiments [1,10], contain saddle points that are not described by the square-root potential (8). Therefore these traps require a separate analysis of the stochastization of motion, although the characteristic energies corresponding to chaotic motion will be in any case close to the potential energy value at the saddle points.

For $E \ll E_s$, when the particle motion in any IQ trap is well described with the idealized IQ trap, the presence of internal nonlinear resonances can lead to chaos. However, the stochastic layers and the stochastic webnet obtained on the basis of possible resonances between the z, ϕ, and ψ motion turn out to be extremely thin. Therefore we neglect for low energies the possibility of stochastization and limit ourselves to the analysis of regular coupling between axial and radial motion.

In our analytical analysis we restrict ourselves to the case $E \ll b \ll 1$ ($\omega_z \ll \omega_\rho$), for which the expansion (14) is valid and the averaging procedure results in Eqs. (26). The most important features of regular coupling between axial and radial motion depend on the ratio between the cubic and fourth-power terms in the expansion of the potential and the ratio of the cubic term to the linear oscillator term for the axial motion. When the condition $\varepsilon \ll 1$ is satisfied both axial and radial motions are dominated by the linear oscillator terms, and the coupling between these motions is weak.

Case (a) (ε_z , $\varepsilon_\rho \ll \varepsilon \ll 1$). In this case the cubic term is the leading nonlinearity, and the fourth-power terms can be neglected in the Hamiltonian, i.e., we may set $B = C = 0$ in Eqs. (26). Then we have J_ψ =const and the equations for J_z, ϕ_z become the following:

$$\dot{J}_z = -A J_\psi J_z^{1/2} \cos\phi_z , \tag{27}$$

$$\dot{\phi}_z = \omega_z + \tfrac{1}{2} A J_\psi J_z^{-1/2} \sin\phi_z . \tag{28}$$

The solution for J_z is

$$J_z \simeq \left\{ \left[\frac{E_z}{\omega_z} + \left(\frac{A J_\psi \sin\phi_z}{2\omega_z} \right)^2 \right]^{1/2} - \frac{A J_\psi \sin\phi_z}{2\omega_z} \right\}^2 . \tag{29}$$

The condition $\varepsilon \ll 1$ is decisive for the behavior of J_z. Since $J_\psi \sim E_\rho/\omega_\rho$, under this condition we have $A^2 J_\psi^2/E_z\omega_z \sim \varepsilon^2 \ll 1$, and

$$J_z \simeq \frac{E_z}{\omega_z} \left(1 - \frac{A J_\psi}{(E_z\omega_z)^{1/2}} \sin\phi_z \right) . \tag{30}$$

This expression clearly shows that the relative change of the action J_z corresponding to the axial motion is small: $\Delta J_z/J_z \sim \varepsilon \ll 1$.

Case (b) ($\varepsilon \gtrsim 1$). In this case $E_z \ll E_\rho$. The representation of a three-dimensional oscillator is still valid. As in the previous case the important features of the

motion originate from the cubic nonlinearity which now dominates over the linear oscillator term for the axial motion. This makes the axial motion strongly nonlinear and causes strong coupling with the radial motion. Large variations of J_z in time can be seen already from Eq. (29), although this equation, based on the averaging procedure, in a strict sense is now valid only up to times $\bar{t} \lesssim 1/\omega_z$. Numerical analysis for large $\omega_z \bar{t}$ shows the same behavior of J_z (see below).

Case (c) ($\varepsilon \ll \varepsilon_z, \varepsilon_\rho$). In this case the fourth-power terms are the dominant nonlinearity and we may set $A = 0$ in Eqs. (26). This limiting case corresponds to an axially symmetric potential and conservation of the angular momentum M along the z axis:

$$M = \left(J_\phi^2 - 4J_\psi^2\right)^{1/2} \sin\psi = \text{const}\,. \tag{31}$$

The equations of motion for J_z and ϕ_z take the form

$$\begin{aligned} \dot{J}_z &= BJ_zJ_\phi \sin 2\phi_z\,, \\ \dot{\phi}_z &= \omega_z - BJ_\phi \sin^2\phi_z\,, \end{aligned} \tag{32}$$

and lead to the following solution for J_z:

$$J_z(\bar{t}) = J_z(0)\left[1 + \frac{\varepsilon_\rho}{2-\varepsilon_\rho} \sin^2[\omega_z\bar{t}(1-\tfrac{1}{2}\varepsilon_\rho)^{1/2}]\right]. \tag{33}$$

Again we arrive at $\Delta J_z/J_z \ll 1$, since the condition $E \ll b$ implies $\varepsilon_\rho \ll 1$.

IV. EXAMPLE

It should be emphasized that even a weak nonlinear coupling, as present in cases (a) and (c), can strongly influence the physical picture of collisionless motion. To illustrate this point we discuss, in particular, how such a coupling causes deformation and disintegration of a small oscillating cloud of atoms in an idealized IQ trap. Related phenomena are observed in experiment [13]. The basic origin of these phenomena is relative dephasing of the oscillations of the atoms. Due to the nonlinear coupling both ω_ρ and ω_z depend on the particle energy. Although this dependence is weak and the particle energies in the cloud differ only slightly, it implies that after many oscillations the atoms no longer move in phase. Dephasing can also result from a slow rotation of the elliptic x,y trajectory (ψ motion), as the associated characteristic frequency ω_ψ strongly depends on the particle energy. These different types of dephasing all result in deformation of the cloud shape and ultimately in the disintegration of the cloud.

We present examples of dephasing in cases (a) and (c), assuming that initially a small cloud of atoms is at rest at a certain position x_0, y_0, z_0 and that the constituent atoms have kinetic energies much smaller than $U_0 = U(x_0, y_0, z_0)$. Under the influence of the potential $U(x, y, z)$ the cloud as a whole will start to move. As $U(x, y, z)$ is almost axially symmetric, the axial angular momentum M of this motion will be close to zero. Calculating $\dot{M}$ using Eqs. (26) (with J_z =const and $\phi_z = \omega_z\bar{t}$) shows that M is oscillating with frequency ω_z and characteristic amplitude $\tilde{M} \sim E_\rho \varepsilon_z^{1/2}/\omega_\rho$. This amplitude is much smaller than the maximum possible value of the angular momentum, E_ρ/ω_ρ, which means that the x, y motion of the atoms occurs along a strongly stretched ellipse with semiminor axis $\sim \varepsilon_z^{1/2} E_\rho^{1/2}/\omega_\rho$. Assuming the semiminor axis to be smaller than the characteristic size of the cloud, we see that initially the cloud will experience two-dimensional oscillations in the ρ,z plane, in combination with a slow ψ motion (rotation around the z axis).

As follows from the equations of motion (26), the frequencies of radial and axial oscillations (averaged over the period of axial oscillations and over the ψ motion) depend on the particle energy and are given by

$$\begin{aligned} \tilde{\omega}_\rho &= \left\langle \frac{\partial \tilde{H}}{\partial J_\phi} \right\rangle = \omega_\rho \left(1 - \frac{3}{8}\varepsilon_\rho - \frac{1}{4}\varepsilon_z\right), \\ \tilde{\omega}_z &= \left\langle \frac{\partial \tilde{H}}{\partial J_z} \right\rangle = \omega_z \left(1 - \frac{1}{4}\varepsilon_\rho\right). \end{aligned} \tag{34}$$

Here we take into account that the amplitudes of radial and axial oscillations remain practically unchanged ($J_\phi = E_\rho/\omega_\rho$ and $J_z = E_z/\omega_z$ are constant), and the average of $\sin^2\psi$ is $\sim \tilde{M}/J_\phi \ll 1$. Expressing $\ddot{J}_\psi$ in terms of J_ψ and M, by using Eqs. (26) averaged over the z motion, the characteristic frequency of the ψ motion is seen to be

$$\tilde{\omega}_\psi \sim 4C\tilde{M} \sim \tfrac{1}{4}\omega_\rho \varepsilon_\rho \varepsilon_z^{1/2}. \tag{35}$$

As the distributions of the radial and axial energies in the cloud have nonzero widths $\delta E_\rho \ll E_\rho$ and $\delta E_z \ll E_z$, the energy dependence of the radial frequency will cause deformation of the cloud shape in the ρ direction. For an initially spherical cloud we have $\delta E_\rho \gg \delta E_z$, and [as follows with Eq. (34)] after a characteristic dephasing time

$$\tau_\rho \sim \frac{2\pi}{\omega_\rho} \frac{b}{\delta E_\rho} \tag{36}$$

the cloud assumes the shape of a pen in the ρ direction with length $2\sqrt{2(U_0 - E_z)}/\omega_\rho$, oscillating along the z axis and having some associated ψ motion. The deformation of this pen in the z direction and that caused by the ψ motion are due to the energy dependences of $\tilde{\omega}_z$ and $\tilde{\omega}_\psi$, and occur much slower than the "pen formation" because $\omega_z \ll \omega_\rho$ and $\varepsilon_z \ll 1$. The corresponding characteristic dephasing times are, respectively,

$$\tau_z \sim \frac{2\pi}{\omega_z} \frac{b}{\delta E_\rho} \sim \tau_\rho \frac{\omega_\rho}{\omega_z} \gg \tau_\rho \tag{37}$$

and

$$\tau_\psi \sim \frac{2\pi}{\omega_\rho \varepsilon_z^{1/2}} \frac{b}{\delta E_\rho} \sim \frac{\tau_\rho}{\varepsilon_z^{1/2}} \gg \tau_\rho. \tag{38}$$

In case (a) we have $\tau_z \ll \tau_\psi$. This means that on a time scale τ_z the pen-shaped cloud will expand in the z direction and acquire the shape of a "vertical" rectangular pancake [with the axial length $2\sqrt{2(U_0 - E_\rho)}/\omega_z$] rotating around the z axis (ψ motion) and slightly twisted as the rotation angle of the ψ motion depends on z. The thickness of the pancake will grow due to dephasing in the ψ motion, and after a time τ_ψ the cloud will be completely disintegrated.

In case (c) the dephasing in the ψ motion occurs much faster than that of the axial oscillations ($\tau_\psi \ll \tau_z$). Accordingly, on a time scale τ_ψ the pen-shaped cloud becomes a "horizontal" pancake oscillating in the z direction. After a time τ_z this pancake expands in the z direction, which completes the disintegration of the cloud.

V. NUMERICAL ANALYSIS

Since the results obtained above analytically for case (a) and case (c) rely on the averaging procedure, they are strictly speaking only justified up to times $\bar{t} \sim \min[1/(\omega_z\varepsilon), 1/(\omega_z\varepsilon_\rho)]$. In order to prove the approximate conservation of J_z and J_ϕ on a much larger time scale we performed numerical calculations using the square-root potential (8) and the procedure of simplectic integrator [14]. Numerically we also obtained results for case (b) and for the stochastic regime.

We first discuss the case $E \ll b \ll 1$. Numerically we arrive for $\varepsilon \ll 1$ at the same conclusions as with our analytical analysis, i.e., the coupling of axial and radial motion is regular and it is small (see Fig. 2). The calculations were performed up to times $\bar{t} \sim 2\pi/\omega_z \times 10^5 \approx 5 \times 10^5$ and showed that J_z and J_ϕ remain approximately constant.

In case (b) our numerical analysis shows strongly nonlinear, but regular, axial motion tightly coupled with the radial motion (see Fig. 3). The relative variations of J_z in time are of order unity. On the contrary, as $E_\rho \gg E_z$, the radial motion remains essentially linear and the variations of J_ϕ are small.

The results obtained for cases (a), (c), and (b) show what can be the characteristic features of optical cooling with a single light beam (parallel to the z axis). If initially the motion corresponds to case (a) or case (c),

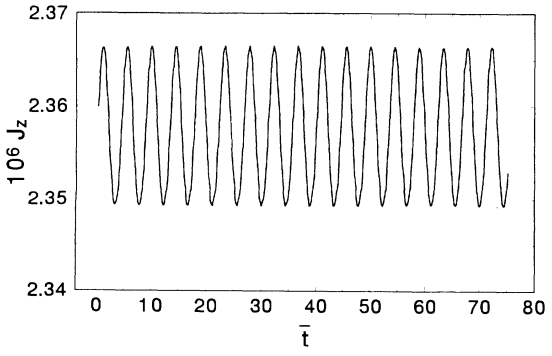

FIG. 2. J_z versus $\bar{t}$ typical for case (a) [$E = 10^{-5}$, $b = 10^{-2}$, $E_z(0)/E = 0.3$].

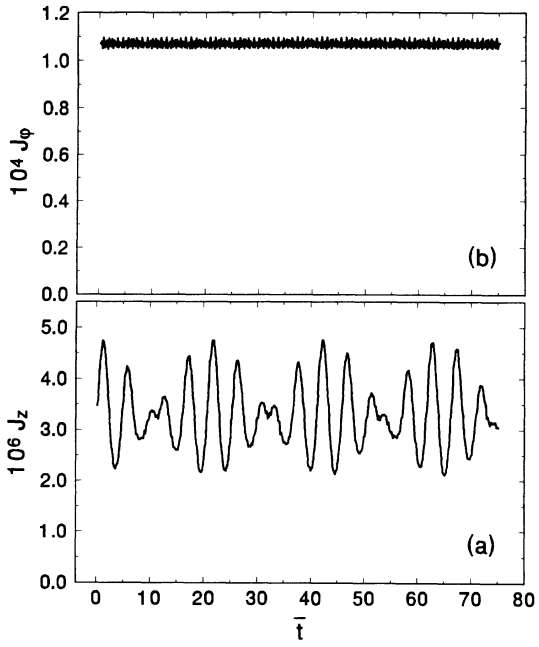

FIG. 3. (a) J_z versus $\bar{t}$ for case (b). (b) J_ϕ versus $\bar{t}$ for case (b). In both cases $E = 10^{-3}$, $b = 10^{-2}$, and $E_z(0)/E = 5 \times 10^{-3}$.

then we first have one-dimensional axial cooling. When the parameter ε (19) increasing in the course of cooling reaches unity, which already corresponds to case (b), the cooling actually becomes three dimensional. Further axial cooling will be accompanied by radial cooling in such a way that $E_z \sim E_\rho^2$ ($\varepsilon \sim 1$).

The variations of J_z and J_ϕ are also small for $b \sim 1$

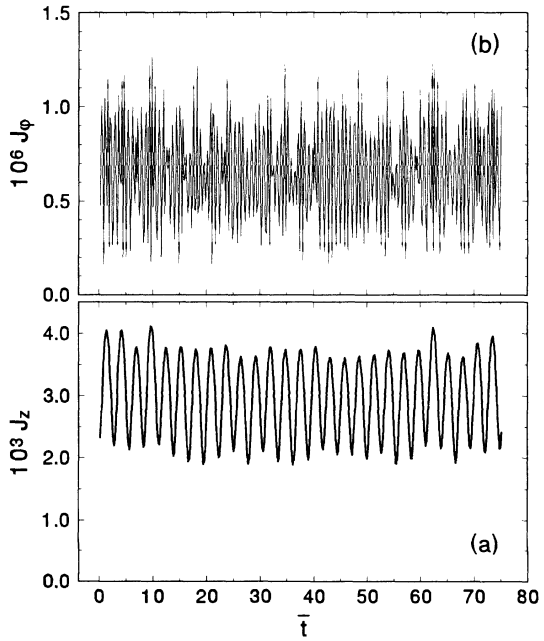

FIG. 4. (a) J_z versus $\bar{t}$ for the case $b \lesssim E \ll 1$. (b) J_ϕ versus $\bar{t}$ for the case $b \lesssim E \ll 1$. In both cases $E = 10^{-2}$, $b = 10^{-3}$, and $E_z(0)/E = 0.35$.

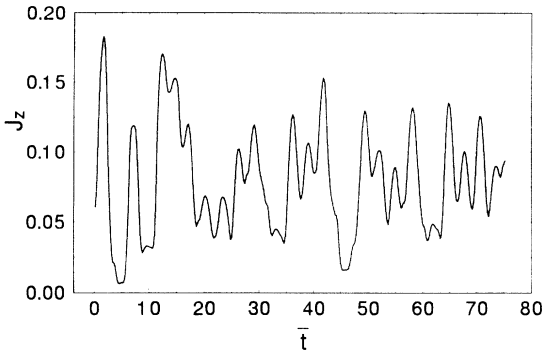

FIG. 5. J_z versus $\bar{t}$ for the case of chaotic motion [E close to $E_s(b)$, $b = 0.1$, $E_z(0)/E = 0.4$].

and $E \ll (1-b)^2$, $\varepsilon \ll 1$, except for b very close to the resonance values 1/3 and 2/3 corresponding to $\omega_z = \omega_\rho$ and $\omega_z = 2\omega_\rho$, respectively. For b outside these narrow resonance regions this case can again be treated as a three-dimensional linear oscillator with a small nonlinear interaction between the degrees of freedom.

The situation is completely different for $b \lesssim E \ll 1$. In this case the motion is fundamentally nonlinear. Numerical analysis shows that the coupling between axial and radial motion is essentially regular as is to be expected for particle motion far from the saddle points. The relative variation of J_z and J_ϕ can be close to unity (see Fig. 4). Notice that for regular coupling it should be possible, at least in principle, to choose the angle-action variables in such a way that the variations of J in time will be small. It should be emphasized that for the present case such a choice will necessarily include a superposition of radial and axial variables, reflecting the fact that there is a significant exchange of energy between the axial and radial degrees of freedom in the course of particle motion.

For energies E close to $E_s(b)$, where the motion should become stochastic, we observe strongly nonregular behavior of $J_z(t)$ (see Fig. 5).

VI. APPROXIMATE ADIABATIC INVARIANTS AND ONE-DIMENSIONAL ADIABATIC COOLING

In this section we analyze the behavior of the system under an adiabatic change of the trapping parameters. We consider the case $\mathcal{E} \ll \mu B_0 \ll \mathcal{E}_c(t)$ [$\Omega_z(t) \ll \Omega_\rho$] assuming that Ω_z is slowly decreasing with increasing time, but Ω_ρ and B_0 remain constant (the trapping parameter α =const and β is decreasing). It is important to realize that even in this case, predominantly corresponding to a weak coupling between the axial and radial degrees of freedom at Ω_z =const, a slow change of Ω_z can cause variations of the action variables and influence the energy exchange between the axial and radial motion.

Since the parameter β is now time dependent, it is reasonable to turn to dimensionless variables (6) where the characteristic quantities l_c, Ω_c, and $\mathcal{E}_c$ are defined with respect to the initial moment of time. Then we arrive at the expansion (14) for the trapping potential $U(\mathbf{r})$ with constant dimensionless radial frequency

$$\omega_\rho = b^{-1/2}, \quad b = \mu B_0/\mathcal{E}_c(0) \ll 1 \tag{39}$$

and time dependent dimensionless axial frequency

$$\omega_z(\bar{t}) = \sqrt{2}\Omega_z(t)/\Omega_z(0) \ll \omega_\rho. \tag{40}$$

Accordingly, the dimensionless nonlinear parameters $\tilde{A}$, $\tilde{B}$, and $\tilde{C}$ will be determined by Eq. (16) with $b \ll 1$ and ω_ρ, $\omega_z(\bar{t})$ from Eqs. (39) and (40).

The condition for an adiabatic change of ω_z is

$$\left|\dot{\omega}_z/\omega_z^2\right| \ll 1. \tag{41}$$

Introducing the ε parameters in the same way as before we see that ε_ρ and ε_z, determining the role of the fourth-power nonlinear terms, are again given by Eq. (18). The expression for the parameter ε coming from the cubic nonlinearity takes the form

$$\varepsilon = \omega_z(\bar{t}) E_\rho E_z^{-1/2}. \tag{42}$$

Turning to angle-action variables in accordance with the canonical transformation (21), (23) we arrive at the Hamiltonian

$$\bar{H} = H + \frac{\dot{\omega}_z(\bar{t})}{2\omega_z(\bar{t})} J_z \sin 2\phi_z, \tag{43}$$

where H is given by Eq. (23) with the parameters A, B, C taken from Eq. (24) and ω_ρ, $\omega_z(\bar{t})$ from Eqs. (39), (40). The second term in Eq. (43) is the time derivative of the generating function of the canonical transformation (21). After averaging over the fast variable ϕ the equations for J_z, ϕ_z take the form

$$\begin{aligned} \dot{J}_z &= -AJ_z^{1/2} J_\psi \cos\phi_z + BJ_z J_\phi \sin 2\phi_z - \frac{\dot{\omega}_z}{\omega_z} J_z \cos 2\phi_z, \\ \dot{\phi}_z &= \omega_z + \tfrac{1}{2} AJ_\psi J_z^{-1/2} \sin\phi_z - BJ_\phi \sin^2\phi_z + \frac{\dot{\omega}_z}{2\omega_z} \sin 2\phi_z, \end{aligned} \tag{44}$$

with $J_\phi = E_\rho/\omega_\rho$ =const.

Analytical analysis of Eqs. (44) is only possible for certain specially selected time dependences $\omega_z(\bar{t})$. Here we do it for the dependence

$$\omega_z(\bar{t}) = \frac{\omega_0}{1 + \bar{t}/\tau} \tag{45}$$

in the limiting case

$$\varepsilon(\bar{t}) \ll \max\left[\frac{1}{\omega_0\tau}, \varepsilon_\rho\right], \tag{46}$$

when the cubic nonlinearity is dominated either by the fourth-power nonlinear terms or by the cooling terms (the last terms) in the right-hand side of Eqs. (44). In this case we may set $A = 0$ in Eqs. (44). Under the condition (41) of adiabatic change of the axial frequency, which for

the time dependence (45) takes the form $\omega_0\tau \gg 1$, the solution for J_z is

$$J_z \simeq J_z(0)\left[1+\left(\frac{1}{(\omega_0\tau)^2}+\tfrac{1}{4}\varepsilon_\rho^2\right)^{1/2} \times \sin^2[\omega_0\tau \ln(1+\bar{t}/\tau)]\right]. \quad (47)$$

Equation (47) shows that the relative variations of J_z in time are small:

$$\frac{\Delta J_z}{J_z} \sim \left(\frac{1}{(\omega_0\tau)^2}+\tfrac{1}{4}\varepsilon_\rho^2\right)^{1/2} \ll 1. \quad (48)$$

Thus J_z is an approximate adiabatic invariant.

In the limit $\varepsilon_\rho \ll 1/\omega_0\tau$ the nonlinear interaction terms in Eqs. (44) are dominated by the cooling terms, and we may set $B = 0$ and, accordingly, $\varepsilon_\rho = 0$ in Eqs. (47) and (48). Physically this means that the change of axial frequency proceeds much faster than the nonlinear coupling between the axial and radial degrees of freedom. In fact, this regime corresponds to one-dimensional cooling of a three-dimensional linear oscillator. In the opposite limit, $\varepsilon_\rho \gg 1/\omega_0\tau$, the fourth-power nonlinear terms are the most important in Eqs. (44). This case is rather close to case (c) in the preceding section. The time dependence of the axial frequency, governed by Eq. (45), only leads to scaling of the time variable. The characteristic variations of J_z remain the same as in the case of constant axial frequency: $\Delta J_z/J_z \sim \varepsilon_\rho \ll 1$.

The approximate conservation of J_z means that the characteristic axial energy $E_z \sim \omega_z$. This implies the phenomena of one-dimensional adiabatic cooling. The radial energy E_ρ =const, and the axial energy decreases directly proportionally to ω_z.

It should be emphasized that under these conditions the parameter ε (42) decreases as $\omega_z^{1/2}(\bar{t})$. This means that the cubic nonlinearity becomes less and less important with increasing $\bar{t}$.

Our analytical analysis was based on the averaging procedure and is, therefore, only valid for a limited time scale. Moreover, the cubic nonlinearity was actually omitted in this analysis. Therefore we undertook a numerical investigation for very long time scales [up to $\bar{t} \sim 10^5/\omega_z(0)$] using the exact (not averaged over ϕ) equations of motion for the square-root potential (8) and several different dependences $\omega_z(\bar{t})$ corresponding to continuously decreasing axial frequency. The calculations show that J_z remains approximately constant (and, hence, E_z continuously decreases proportionally to ω_z) as long as condition (41) is satisfied. The latter is violated beyond a certain time if ω_z is reduced faster than $1/\bar{t}$. These calculations also include the cases when the cubic nonlinearity is important at least in the initial stage of the cooling process.

Numerical analysis was also done for the situation where ω_z is decreasing only during a certain period of time τ and then remains constant. The calculations show that the quantity $[J_z(\infty) - J_z(0)]/J_z(0) \ll 1$ if $\tau\omega_z(\bar{t}) \gtrsim 1$ (see Fig. 6).

It should be emphasized that one-dimensional adiabatic cooling is also possible for energies $1 \gg E \gtrsim b$. Since $b \ll 1$, the axial oscillations in this case again proceed much slower than the radial ones. It means that the axial motion can be represented as the motion in the effective potential which is the sum of the trapping potential and the radial kinetic energy, both averaged over the radial oscillations. During the period of axial oscillations a substantial transformation of energy between axial and radial degrees of freedom takes place, and in this sense one can say that these motions are tightly coupled. At the same time, our numerical analysis shows that the axial kinetic energy averaged over axial and radial oscillations monotonously decreases with adiabatically decreasing parameter β (at constant α and B_0), the averaged radial kinetic energy remaining approximately unchanged.

The results obtained clearly show a realistic possibility for one-dimensional adiabatic cooling of magnetically trapped atomic gases in the collisionless regime. This is an interesting option for light atoms, such as hydrogen and antihydrogen, as they have relatively high optical cooling limits (~10 mK) [15]. In particular, this option may be valuable for gravity experiments with antihydro-

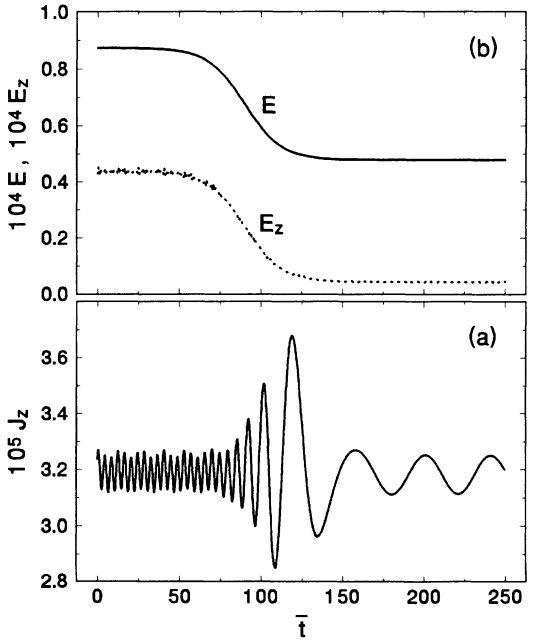

FIG. 6. Example of axial adiabatic cooling with ω_ρ =const; $\omega_z(\bar{t}) = \frac{1}{2}[\omega_z(0)+\omega_z(\infty)] - \frac{1}{2}[\omega_z(0)-\omega_z(\infty)]\tanh[(\bar{t}-\bar{t}_0)/\tau]$; $\omega_z(0) = \sqrt{2}$, $\omega_z(\infty) = 0.1\,\omega_z(0)$, $\tau = 50$, $\bar{t}_0 = 110$. (a) J_z versus $\bar{t}$. (b) E_z and E versus $\bar{t}$.

gen [4], which require (vertical) temperatures in the microkelvin range. Such temperatures have been achieved for hydrogen with the evaporative cooling method [1], but the required densities may be difficult to realize for antihydrogen. In this respect one-dimensional cooling is a promising option, which could be tested in experiments with hydrogen atoms.

ACKNOWLEDGMENTS

We acknowledge fruitful discussions with T. Bergeman, Yu.A. Danilov, and T.W. Hijmans. This research was supported by the Nederlandse Organisatie voor Wetenschappelijk Onderzoek (NWO-PIONIER and NWO-07-30-002).

[1] D.M. Doyle, J.C. Sandberg, I.A. Yu, C.L. Cesar, D. Kleppner, and T.J. Greytak, Phys. Rev. Lett. **67,** 603 (1991).

[2] C.R. Monroe, E.A. Cornell, S.A. Sackett, C.J. Myatt, and C.E. Wieman, Phys. Rev. Lett. **70**, 414 (1993).

[3] G.V. Shlyapnikov, J.T.M. Walraven and E.L. Surkov, Hyperfine Interact. **76,** 31 (1993).

[4] *Antihydrogen*, edited by J. Eades (Baltzer, Basel, 1993) [originally published as special issues of Hyperfine Interact. **76** (1–4) (1993)].

[5] T.H. Bergeman, P. McNicholl, J. Kycia, H.J. Metcalf, and N.L. Balazs, J. Opt. Soc. Am. B **6**, 2249 (1989).

[6] T. Bergeman, G. Erez, and H.J. Metcalf, Phys. Rev. A **35**, 1535 (1985).

[7] By regular coupling between the degrees of freedom we mean the coupling which does not lead to chaotization of motion, i.e., trajectories initially close in the phase space do not diverge exponentially with increasing time. Roughly speaking, regular coupling takes place when the share of noise admixture is small in comparison with regular component of motion. In this case we have regular exchange of energy between the degrees of freedom.

[8] Y.V. Gott, M.S. Ioffe, and G.V. Tel'kovski, Nucl. Fusion, 1962 Suppl., Pt. 3, 1045 (1962).

[9] D.E. Pritchard, Phys. Rev. Lett. **51,** 1336 (1983).

[10] O.J. Luiten, H.G.C. Werij, I.D. Setija, M.W. Reynolds, T.W. Hijmans, and J.T.M. Walraven, Phys. Rev. Lett. **70,** 544 (1993).

[11] G.E.O. Giacaglia, *Perturbation Methods in Non-linear Systems* (Springer, Berlin, 1972).

[12] G.M. Zaslavsky, R.Z. Sagdeev, D.A. Usikov, and A.A. Chernikov, *Weak Chaos and Quasi-Regular Patterns*, Cambridge Nonlinear Science Series Vol. 1 (Cambridge University Press, Cambridge, England, 1991).

[13] R. J. C. Spreeuw, C. Gerz, L. S. Goldner, W. D. Phillips, S. L. Rolston, C. I. Westbrook, M. W. Reynolds, and I. F. Silvera, Phys. Rev. Lett. **72**, 3162 (1994).

[14] H. Kinoshita, H. Yoshida, and H. Nakai (unpublished).

[15] J.T.M. Walraven, Hyperfine Interact. **76**, 205 (1993).